

ULRR

Damage modelling of fibre reinforced polymer matrix composite open hole tension specimens using the Ladevèze damage model in Pam-CRASH

Item Type	Report
Authors	O'Higgins, Ronan;McCarthy, Michael A.;McCarthy, Michael
Download date	2026-06-13 03:38:03
Item License	https://creativecommons.org/licenses/by-nc-sa/1.0/
Link to Item	https://hdl.handle.net/10344/5009

Technical Report for ESI Group

**Damage Modelling of Fibre Reinforced Polymer
Matrix Composite Open Hole Tension Specimens
using the Ladevèze Damage Model in Pam-CRASH**

Mr. Ronan O'Higgins, Prof. Michael McCarthy

Department of Mechanical and Aeronautical Engineering
University of Limerick,
Limerick,
Republic of Ireland



University of Limerick

Contents

1	Introduction	3
2	Experimental Determination of Ladevèze Damage Model Parameters	4
2.1	General Experimental Methods	4
2.2	Results and Discussion	7
2.3	Conclusion	19
3	Calibration of Composite Open Hole Tension Ladevèze Damage Model in Pam-CRASH	21
3.1	Model Properties	21
3.2	Parameter Studies	23
3.3	Delamination Modelling	29
4	Conclusions and Recommendations	31
5	References	32
6	Acknowledgements	33

Section 1: Introduction

The goal of this project was to accurately predict the ultimate failure strengths of fibre reinforced polymer matrix composite open hole tension specimens using the Ladevèze continuum mechanics damage model, currently available within the ESI Group Pam-CRASH software, using input parameters experimentally derived at the University of Limerick.

This report presents the work carried out at the University of Limerick, both experimental and numerical, as part of the project. Results of an experimental test series carried out to derive Ladevèze damage model parameters for a carbon fibre reinforced polymer matrix composite are presented and discussed. In addition, the results of a numerical study carried out to calibrate the Ladevèze damage model, used to predict the ultimate strength of fibre reinforced open hole tension specimens are presented and discussed.

Section 2 presents the procedures used and results of an experimental test series to derive Ladevèze damage model parameters. Section 3 presents the numerical work carried out at the University of Limerick as part of this project.

Section 2: Experimental Determination of Ladevèze Damage Model Parameters

The aim of this section is to present the results of an experimental study carried out to determine the Ladevèze damage parameters of HTA 6376 carbon fibre reinforced plastic, (CFRP) for use in numerical analysis work. The theory behind the model is not explained, however, equations needed to determine the damage parameters are presented. The procedure follows that devised by Ladevèze and Le Dantec [1]. Four different tests were carried out to determine basic material properties and the Ladevèze damage parameters. For ease of explanation the procedure and results for each test are dealt with in their own separate sub-sections.

2.1 General Experimental Methods

2.1.1 Test Plan

The general test geometry is shown in Figure 2.1. The test procedure and coupon geometry are dependent on the specific properties, which the coupon is being used to determine. As these tests were devised by the developers of the Ladevèze model to determine specific material characteristic model inputs they are not standardised by any industrial standards body. However, for this test series, tensile testing was carried out, where possible, in accordance ASTM standard D3039/D3039M – 00, “Standard Test Method for Tensile Properties of Polymer Matrix Composite Materials” [2].

The material studied in this test series is Hexcel Materials Ltd. 6376C-HTA(12K)-5.5-29.5% carbon fibre reinforced plastic (CFRP). Details on specimen lay-up and geometry are given in table 2.1.

2.1.2 Specimen Preparation and Testing

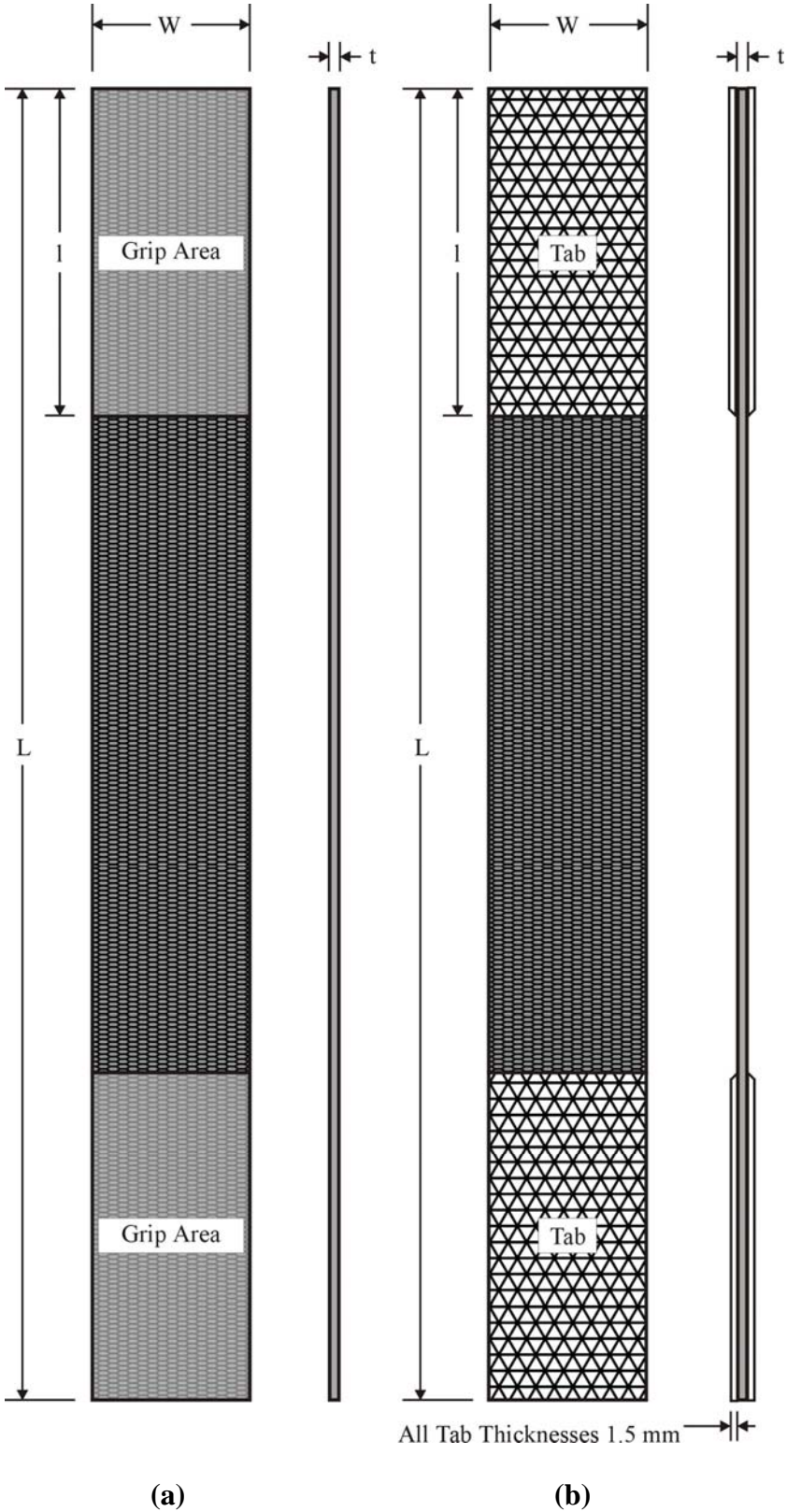
All test specimens were prepared at the University of Limerick from preimpregnated rolls of material according to manufacturer guidelines and ASTM standards [2, 3]. Testing was performed on a Zwick/Roell 100kN universal straining frame equipped with hydraulic grips. For tests involving specimens that had an ultimate load of less than 10kN, a 10kN load cell was attached to the straining frame. All tests were conducted at a machine head displacement rate of 0.03 mm/s (approximately 2 mm/min.) according to ASTM standard D3039/D3039M - 00 [2]. All specimens were instrumented with either Epsilon axial extensometers or an Epsilon biaxial extensometer, depending on the need to measure strain in either one or more directions. In addition at least one of each type of test specimen was instrumented with strain gauges to verify the results being obtained from the extensometers.

2.1.3 Common Equations

The following common equations were used to calculate stress and strain in the direction of loading for all specimens geometries. Stress was calculated in accordance with ASTM Standard D3039/D3039M –00 [2] from:

$$\sigma_i = \frac{P_i}{A} \quad (2.1)$$

where: $\sigma_i =$, stress at the i -th data point, $P_i =$ load at i -th data point, and A is the specimen average cross sectional area.



Notes: 1. l – grip length or tab length, this dimension is 75 mm for all Test Series 2 specimens.
2. Dimensions for the specimens are given in Tables 3 and 4

Figure 2.1, Ladevèze test specimen geometry (a) without tabs, (b) with tabs

Table 2.1 Test Matrix

Code	Lay-up	Loading	Specimen Geometry				Instrumentation	Primary Output	Test Loading		
			L (total)	w	t	Tabs			Failure	Linear Elastic Region	Total
L_C_0_T#	(0) ₈	Tension	250	15	1	Yes	Strain Gauged/ Extensometers	$E_1, \nu_{12}, S_{11}, \epsilon_{11}$	5	0	5
L_C_PM45_T#	(45/-45) _{2s}	Tension	250	25	1	No	Strain Gauged/ Extensometers	$G_{12}, S_{12},$ Damage Parameters	0	5 cyclic (6 cycles)	5
L_C_P45_T#	(45) ₈	Tension	250	25	1	No	Strain Gauged/ Extensometers	Damage Parameters	2	3 cyclic (6 cycles)	5
L_C_PM67_T#	(67.5/-67.5) _{2s}	Tension	250	25	1	No	Strain Gauged/ Extensometers	Damage Parameters	2	3 cyclic (6 cycles)	5
Total									9	11	20

- All test specimens are manufactured from 6376C-HTA(12K)-5.5-29.5% CFRP Prepreg
- All specimen dimensions are given in millimetres
- Symbols: # - Test Number E – Young’s Modulus G – Shear Modulus ν – Poisson’s Ratio
 S – Ultimate Strength ϵ - Ultimate Strain L – Length w – Width
 t - thickness
- Subscripts: () - Number of plies in Laminate $1, 2, 3$ – Material Principal Axes
()_s – Laminate is symmetric

In accordance with the standard [2], the average cross sectional area, A , is the product of the average of three thickness measurements along the gauge length of the specimen, and the average of three width measurements taken along the gauge length of the specimen. The ultimate strength, S , of the specimen is defined as the stress calculated from the maximum load, P^{max} , before failure.

In accordance with ASTM standard D3039/D3039M –00 [2], strain was calculated from:

$$\varepsilon_i = \frac{\delta_i}{L_g} \quad (2.2)$$

where: ε_i = strain at the i -th data point, δ_i = gauge length displacement at the i -th data point, L_g = initial gauge length. The ultimate strain, e , is the strain at which ultimate failure occurs.

2.2 Results and Discussion

The presentation of results is divided into a number of sections. Each section looks at the procedure and results of an individual test method used to calculate specific Ladevèze damage parameters. Section 2.2.1 presents the results of tests on 0° coupons to determine fibre tensile elastic and limit properties. Section 2.2.2 presents the results of cyclic tensile tests on $\pm 45^\circ$ coupons to determine the Ladevèze model shear damage and plasticity parameters. Finally Sections 2.2.3 and 2.2.4 present results for cyclic tensile tests on $\pm 67.5^\circ$ and 45° coupons respectively, used to determine the Ladevèze model transverse damage and coupling parameters.

2.2.1 Fibre Direction Tensile Properties

Quasi- static tensile tests were carried out on 0° coupons, according to ASTM Standard D3039/D3039M –00 [2], to determine the elastic tensile material properties in the fibre direction, E_{11} and ν_{12} , and also the fibre limit properties, e_{11} and S_{11} . The results and full stress-strain curve for the HTA 6376 specimens are reproduced here in Table 2.2 and Figure 2.2.

Table 2.2 HTA 6376 CFRP tensile properties in the fibre direction

Material Properties	E_{11} (GPa)	ν_{12}	S_{11} (MPa)	e_{11} (%)
\bar{x}	133	0.32	2170	1.506
s_{n-1}	3.41	0.017	109.6	0.014
CV (%)	2.56	5.15	5.05	0.93

The stress-strain curve presented in Figure 2.2 clearly shows that the stiffness of the 0° specimen remains constant to failure, i.e. no non-linearity is apparent in the stress-strain curve. It is for this reason that the Ladevèze model assumes that there is no plasticity in the fibre direction, rather the fibre behaviour in tension tends to be brittle linear elastic behaviour.

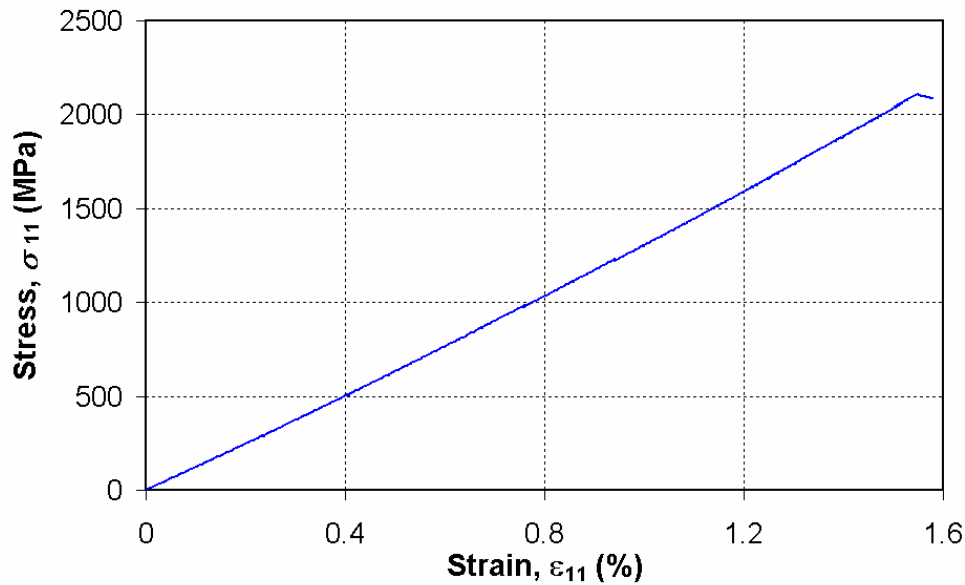


Figure 2.2 A typical HTA 6376 CFRP 0° tension specimen stress-strain curve to failure

2.2.2 Determination of Shear Damage and Plasticity Parameters from Cyclic Tensile Testing of $\pm 45^\circ$ Specimens

The Ladevèze model characterizes damage by material stiffness loss. This is revealed by elastic modulus variations on the experimental curves. Plasticity is revealed by the emergence of permanent strains. Plasticity and shear damage (fibre/matrix debonding) parameters are determined by carrying out cyclic tensile tests on $\pm 45^\circ$ specimens of the material system of interest. The $\pm 45^\circ$ specimen was chosen to determine the shear properties as the $\pm 45^\circ$ fibre alignment provides reinforcement in the transverse direction in each individual ply of the laminate keeping transverse strains and damage to negligible levels. Similarly, strains in the fibre direction of these specimens are kept to negligible levels as shearing and fibre/matrix debonding prevents any large strains being induced in the fibres. In this study cyclic tensile tests refers to cyclic loading of specimens consisting of loading and unloading the specimen with the amplitude of displacement increased for each cycle. The number of cycles does not exceed five or six in order to stay in a domain where low-cycle fatigue phenomena are negligible. Figure 2.3 shows a typical example of a stress-strain curve for this sort of cyclic loading. E_0 represents the initial undamaged modulus of the specimen. E_i represents the reduced modulus of the damaged specimen at the i -th loading/unloading cycle. E_i is calculated from:

$$E_i = \frac{\sigma_i}{\epsilon_{ei}} \quad (2.3)$$

where: σ_i = peak stress for the i -th loading/unloading cycle, and ϵ_{ei} = elastic part of the total peak strain for the i -th loading/unloading cycle. The total strain, ϵ_{i}^T , is the peak strain reached by the specimen for an i -th loading/unloading cycle and consists of elastic strain, ϵ_{ei} , and when permanent deformation occurs in the specimen, plastic strain, ϵ_{pi} . The plastic strain for an i -th loading/unloading cycle is defined as the permanent strain recorded after the specimen has been unloaded to zero load at the end of a cycle. Elastic strain for an i -th

loading/unloading cycle is defined as the total peak strain of the cycle, ε_i^T , minus the plastic strain for the cycle, ε_{pi} , as shown in Figure 2.3.

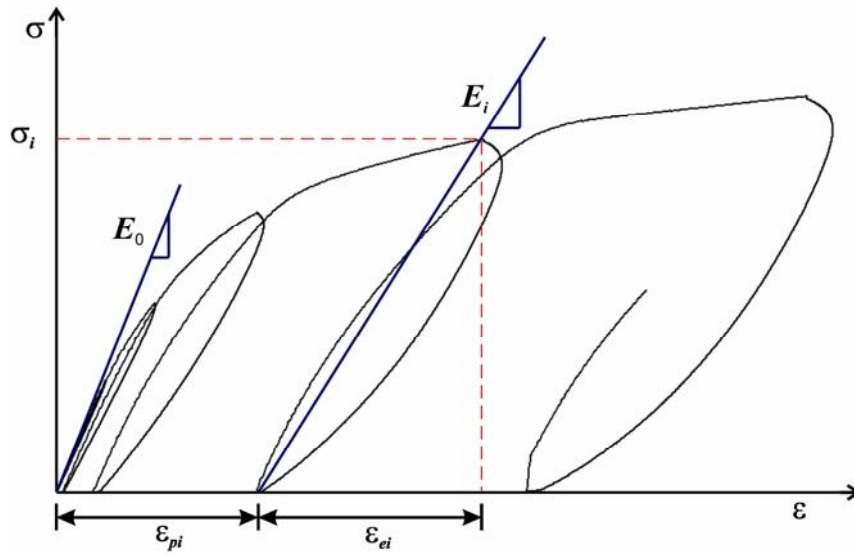


Figure 2.3 Damage measurement and plastic strain measurement

For the $\pm 45^\circ$ specimens, the properties of interest are shear stress, τ_{12} , shear strain, γ_{12} , and shear modulus, G_{12} . Each $\pm 45^\circ$ specimen tested was instrumented with a biaxial extensometer to measure strains in the specimen longitudinal and transverse directions. Load was recorded using a 10kN load cell. The shear stress for the $\pm 45^\circ$ specimen was calculated according to Ladevèze and Le Dantec [1] from:

$$\tau_{12i} = \frac{\sigma_{Li}}{2} \tag{2.4}$$

where: τ_{12i} = shear stress at the i -th data point, and σ_{Li} = specimen stress at the i -th data point calculated according to equation 2.1.

The shear strain in a $\pm 45^\circ$ specimen was calculated according to Ladevèze and Le Dantec [1] from:

$$\gamma_{12i} = \varepsilon_{Li} - \varepsilon_{Ti} \tag{2.5}$$

where: γ_{12i} = shear strain at the i -th data point, ε_{Li} = specimen longitudinal strain at the i -th data point, and ε_{Ti} = specimen transverse strain at the i -th data point.

Figure 2.4 shows a typical shear stress-shear strain curve for a cyclic Ladevèze test on an HTA 6376 CFRP $\pm 45^\circ$ specimen. A number of such tests were carried out to determine the Ladevèze shear damage and plasticity parameters. The displacement amplitude was varied for each cycle and for each specimen to give a wide range of data for use in calculating the damage and plasticity parameters. One specimen was tested with a range of very small displacements to determine at what stress/strain permanent strains were induced in the specimen.

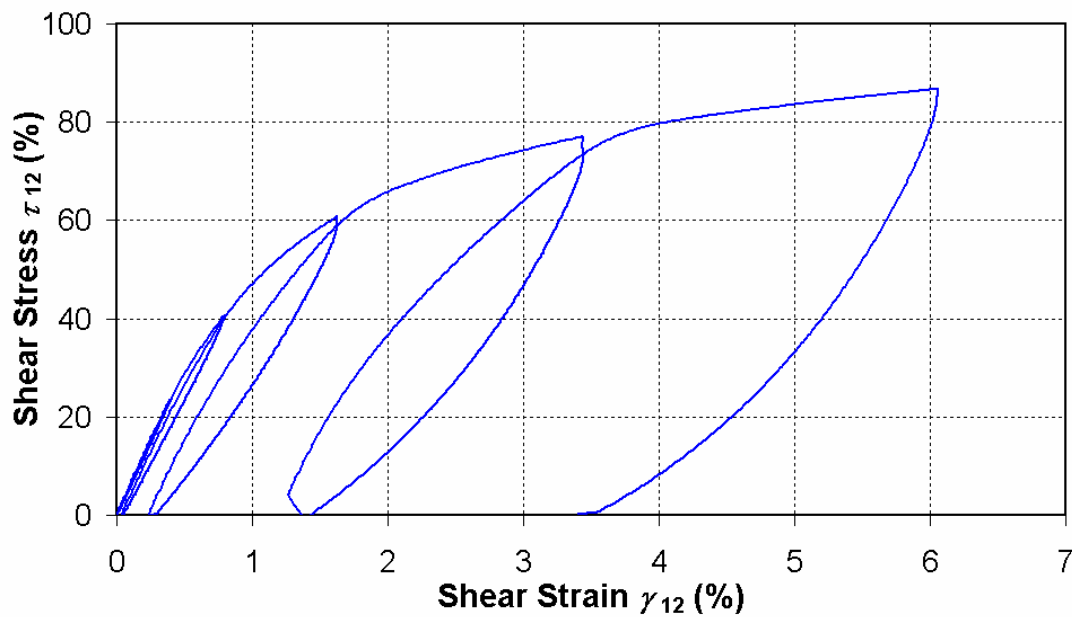


Figure 2.4 A Typical HTA 6376 CFRP ±45° specimen cyclic Ladevèze test shear stress-shear strain curve

For each cycle, the elastic and permanent strains induced in the specimen were determined. In addition, the shear modulus, G_{12} , of each cycle was also calculated in accordance with the method outlined above. Once the shear modulus for each of the cycles had been calculated, the individual scalar shear damage variable, d , was calculated for each cycle from:

$$d_i = 1 - \frac{G_{12i}}{G_{12_0}} \tag{2.6}$$

where: d_i = scalar shear damage variable for the i -th test cycle, G_{12i} = shear modulus for the i -th test cycle, and G_{12_0} = initial undamaged specimen shear modulus.

Having calculated d for each cycle, the damage development law quantity \underline{Y} can be calculated for each loading/unloading cycle of the ±45° specimen from:

$$\underline{Y}_i = \sqrt{Y_{di}} = \frac{\tau_{12i}}{(1 - d_i)\sqrt{2G_{12_0}}} \tag{2.7}$$

where: \underline{Y}_i = damage development law quantity \underline{Y} for the i -th test cycle, τ_{12i} = peak shear stress for the i -th test cycle, d_i = scalar shear damage variable for the i -th test cycle, and G_{12_0} = initial undamaged specimen shear modulus.

Having determined both \underline{Y} and d for each test cycle, they can be plotted against each other as shown in Figure 2.5, a linear approximation fitted through the data forms the elementary ply shear damage master curve.

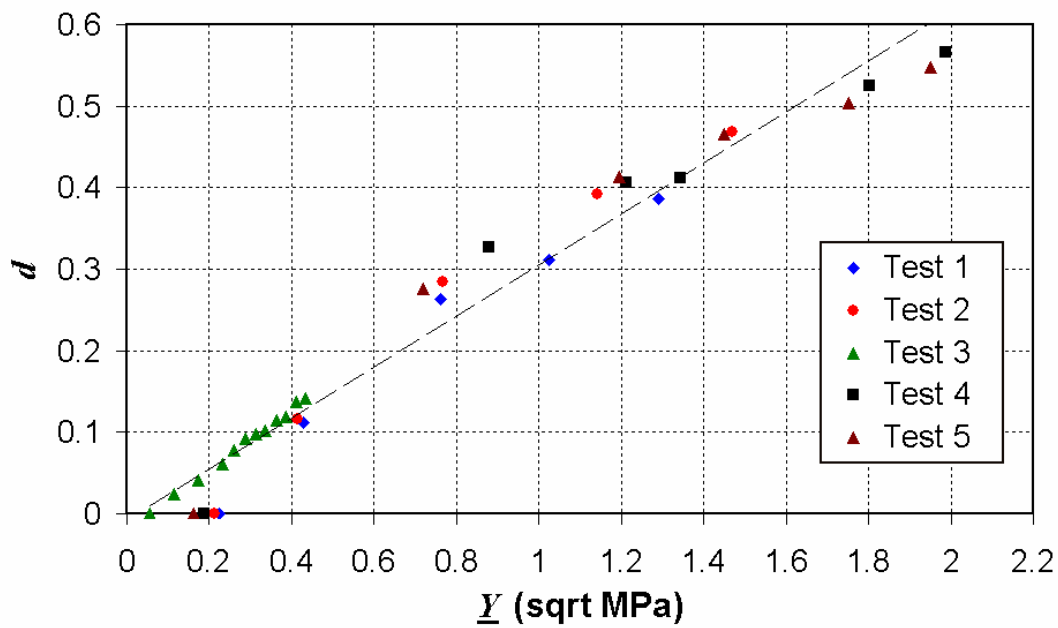


Figure 2.5 Shear damage master curve for an elementary ply of HTA 6376 CFRP, determined from $\pm 45^\circ$ specimen cyclic Ladevèze tests

The shear damage master curve can be expressed by the equation:

$$d_i = \frac{Y_i - Y_0}{Y_c} \tag{2.8}$$

where: Y_0 = initial shear damage threshold value, and Y_c is the critical shear damage limit value. Table 2.3 shows the values of Ladevèze damage model input parameters Y_0 and Y_c for an elementary ply of the HTA 6376 CFRP material system.

Table 2.3 Ladevèze model shear damage master curve constants for HTA 6376 CFRP.

Material System	Y_0 ($\sqrt{\text{MPa}}$)	Y_c ($\sqrt{\text{MPa}}$)
HTA 6376	0.048	3.10

The Ladevèze model plasticity development law parameters can also be determined from the data obtained in the cyclic tests of the $\pm 45^\circ$ specimens. The threshold values ($R+R_0$) can be calculated from:

$$R_i + R_0 = \frac{\tau_{12i}}{(1 - d_i)} \tag{2.9}$$

where R_i = plasticity development law parameter for the i -th test cycle, R_0 is the initial yield stress and the other symbols have the usual meaning.

The accumulated plastic strain, p , is calculated from the following integration:

$$p = \int_0^{\gamma_{p12}} (1 - d) \delta \varepsilon \tag{2.10}$$

where: γ_{p12} = plastic part of the total shear strain, and the other symbols have the usual meaning.

Having determined both $(R+R_0)$ and p , they are plotted against one another as shown in Figure 2.6 to determine the elementary ply master curve. A parabolic curve can be plotted through the data shown in Figure 2.6 to take the form:

$$R(p) = \beta p^m \tag{2.11}$$

where: β = plasticity development law multiplier, m = plasticity development law exponent, and the other symbols have the usual meaning. Table 2.4 gives values of R_0 , b and m for both HTA 6376 CFRP determined from the test data.

Table 2.4 Ladevèze model plasticity master curve constants for HTA 6376 CFRP.

Material System	R_0 ($\sqrt{\text{MPa}}$)	β ($\sqrt{\text{MPa}}$)	m
HTA 6376	21.59	558	0.38

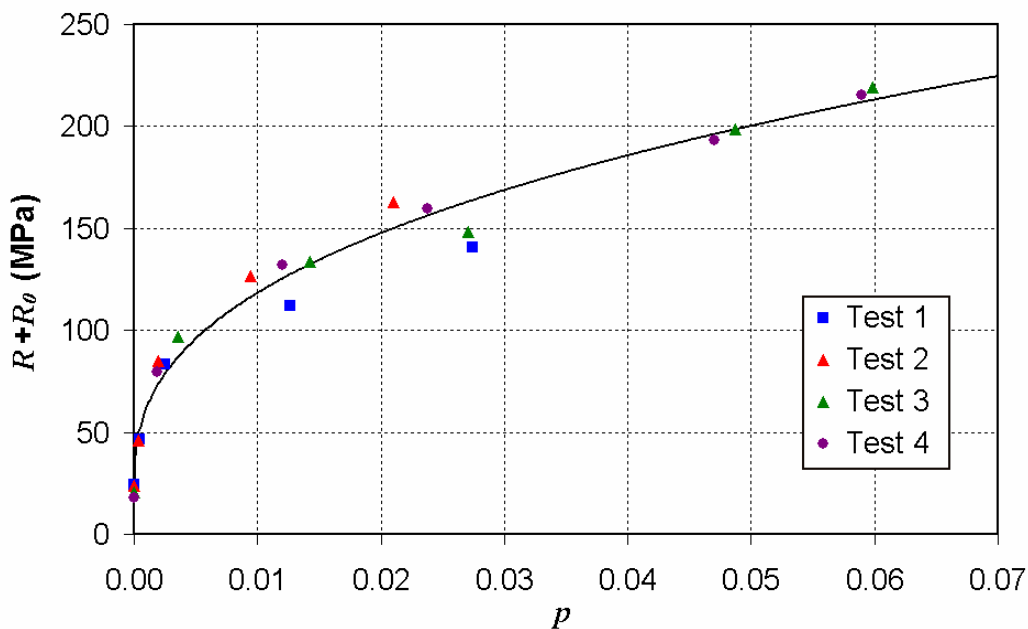


Figure 2.6, Plasticity master curve for an elementary ply of HTA 6376 CFRP, determined from $\pm 45^\circ$ specimen cyclic Ladevèze tests.

2.2.2 Determination of Transverse Damage and Coupling Parameters from Cyclic Tensile Testing of $\pm 67.5^\circ$ Specimens

Cyclic tensile tests are carried out on $\pm 67.5^\circ$ specimens to determine Ladevèze model transverse damage parameters (matrix microcracking) and shear damage/transverse damage coupling parameters. The $\pm 67.5^\circ$ specimen is used for this purpose, as it is possible to accurately determine both transverse and shear strains in the elementary plies of the specimen from the longitudinal and transverse strains of the overall specimen. In addition, the alignment of the fibres does not hinder the progress of damage in the transverse direction, as is the case for the $\pm 45^\circ$ specimen, and the off-axis angle of fibre alignment allows sufficient shear damage to occur so that coupling parameters between the two damage mechanisms can be determined. For this test both the transverse and shear material properties are of interest. For an angle ply tensile test such as this, the material properties are calculated according to classical laminate theory from the following equations:

$$\sigma_{22} = (1 - B)\sigma_L \quad (2.12)$$

$$\tau_{12} = \frac{-1}{2mn} (B(1 - 2m^2) + m^2)\sigma_L \quad (2.13)$$

where

$$B = \left[\frac{m^2(2m^2 - 1) + 4m^2n^2 \frac{G_{12-0}}{E_{22-0}} \left(\frac{E_{22-0}}{E_{11}} \nu_{12} + 1 \right)}{4m^2n^2 \frac{G_{12-0}}{E_{22-0}} \left(\frac{E_{22-0}}{E_{11}} + 2 \frac{E_{22-0}}{E_{11}} \nu_{12} + 1 \right) + (2m^2 - 1)(m^2 - n^2)} \right] \quad (2.14)$$

σ_L = specimen longitudinal stress calculated according to equation 2.1, $m = \cos \theta$, $n = \sin \theta$, and the other symbols have the usual meaning. For a $\pm 67.5^\circ$ specimen of HTA 6376 CFRP B was found to be 0.256.

The strains in the principal material coordinates of interest can be calculated from:

$$\varepsilon_{22} = n^2 \varepsilon_L + m^2 \varepsilon_T \quad (2.15)$$

$$\gamma_{12} = -2nm(\varepsilon_L - \varepsilon_T) \quad (2.16)$$

where the symbols have the usual meaning.

Using equations 2.12 to 2.16, the shear and transverse responses of the $\pm 67.5^\circ$ specimen were plotted as shown in Figures 2.7 and 2.8 respectively.

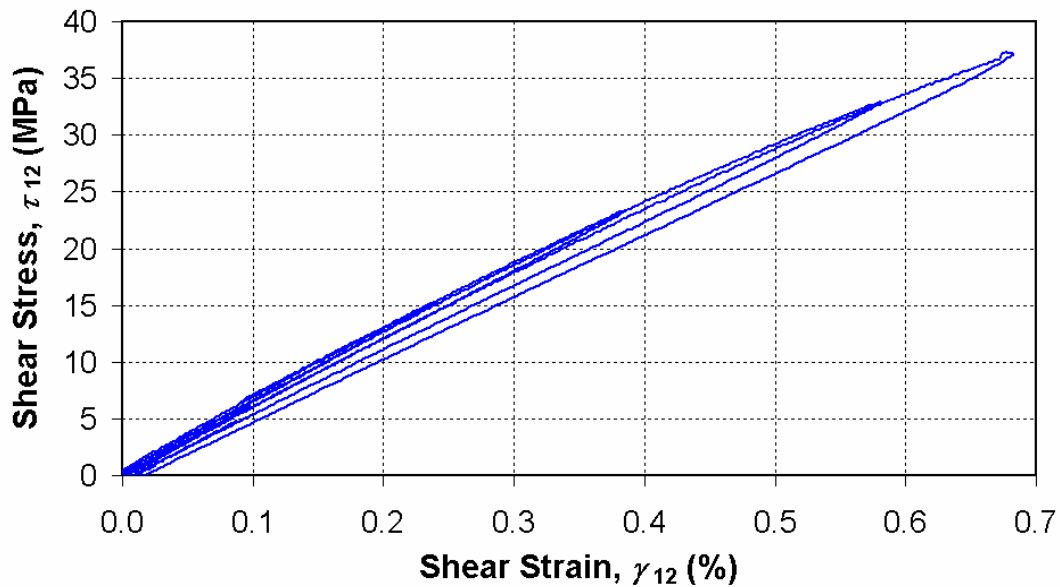


Figure 2.7, Typical shear behaviour for a cyclic tensile test on a HTA 6376 CFRP $\pm 67.5^\circ$ specimen.

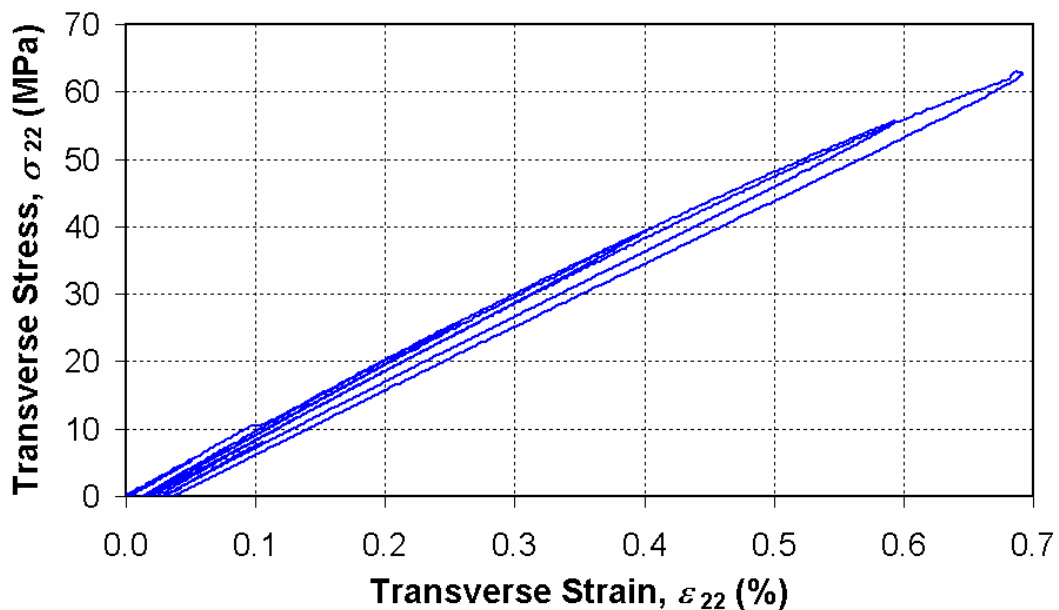


Figure 2.8, Typical transverse behaviour for a cyclic tensile test on a HTA 6376 CFRP $\pm 67.5^\circ$ specimen.

For each cycle, the elastic and permanent strains induced in the specimen were determined. In addition, the shear modulus, G_{12} , and transverse modulus, E_{22} , of each cycle were also calculated in accordance with the method outlined in Section 2.2.2. Once the shear and transverse moduli for each of the cycles had been calculated, the scalar shear damage

variable, d , and scalar transverse damage variable, d' , were calculated for each cycle. The d variable was calculated according to equation 2.8, similarly d' was calculated from:

$$d'_i = 1 - \left(\frac{E_{22i}}{E_{22_0}} \right) \quad (2.17)$$

where: d'_i = scalar transverse damage variable for the i -th load cycle, E_{22i} = ply transverse modulus for the i -th load cycle, E_{22_0} = initial ply transverse modulus of the specimen.

Having calculated the scalar shear and transverse damage variables for the specimen, the damage functions Y_d and $Y_{d'}$ are calculated from:

$$Y_d = \frac{1}{2} \frac{\tau_{12}^2}{G_{12_0} (1-d)^2} \quad (\text{shear damage}) \quad (2.18)$$

$$Y_{d'} = \frac{1}{2} \frac{\sigma_{22}^2}{E_{22_0} (1-d')^2} \quad (\text{transverse damage}) \quad (2.19)$$

where the symbols have the usual meaning.

The shear damage/transverse damage coupling factor b was then be calculated from:

$$b = \frac{(Y_c d + Y_0)^2 - Y_d}{Y_{d'}} \quad (2.20)$$

where: Y_c = critical shear damage limit value obtained from the $\pm 45^\circ$ specimen tests (see Table 2.3), d = scalar shear damage variable, Y_0 = initial shear damage threshold value obtained from the $\pm 45^\circ$ specimen tests (see Table 2.3). Y_d and $Y_{d'}$ are the shear and transverse damage functions, respectively.

It is now possible to calculate the damage development law function \underline{Y} for transverse damage from:

$$\underline{Y} = \sqrt{Y_d + bY_{d'}} \quad (2.21)$$

where the symbols have the usual meaning.

Figure 2.9 shows the linear approximation, fitted to the experimental data, of the transverse damage master curve of an elementary ply HTA 6376 CFRP.

The transverse damage master curve can be expressed by the equation:

$$d'_i = \frac{Y_i - Y'_0}{Y'_c} \quad (2.22)$$

where: Y'_0 = initial transverse damage threshold value, Y'_c is the critical transverse damage limit value and where \underline{Y}_i and d'_i have the usual meaning. Table 2.5 shows the values of Y'_0 and Y'_c for an elementary ply of HTA 6376 CFRP.

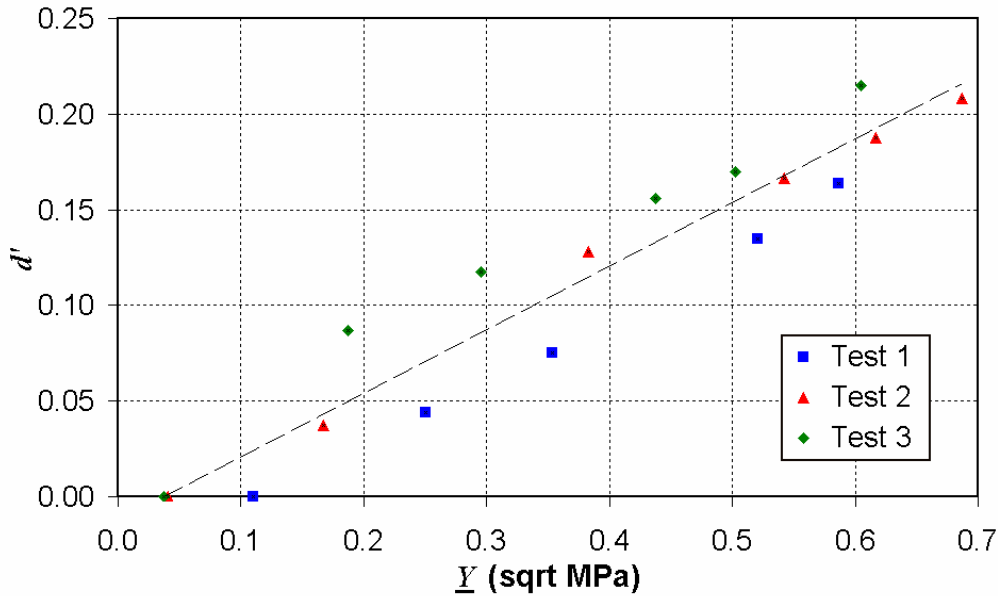


Figure 2.9 Transverse tension damage master curve for an elementary play of HTA 6376 CFRP derived from $\pm 67.5^\circ$ specimen tests

Table 2.5 Ladevèze model transverse damage master curve constants

Material System	Y'_0 ($\sqrt{\text{MPa}}$)	Y'_c ($\sqrt{\text{MPa}}$)
HTA 6376	0.07	2.75

Finally, the plasticity coupling factor a^2 was calculated from:

$$a^2 = \frac{\epsilon_{p22}(1-d')^2 \tau_{12}}{\gamma_{p12}(1-d')^2 \sigma_{22}} \tag{2.23}$$

where the symbols have the usual meaning. The damage and plasticity coupling factors for an elementary ply of HTA 6376 CFRP are given in Table 2.6.

Table 2.6 Ladevèze model damage and plasticity coupling factors

Material System	b	a^2
HTA 6376	0.53	0.54

2.2.4 Determination of Transverse Damage and Coupling Parameters from Cyclic Tensile Testing of 45° Specimens

Ladevèze cyclic tensile testing of 45° off-axis specimens is an alternative method to the $\pm 67.5^\circ$ cyclic test for determining transverse damage and coupling parameters. Figures 2.10 and 2.11 show typical Ladevèze 45° off-axis specimen transverse stress-strain curves and shear stress-strain curves for HTA 6376 CFRP. Both figures show similar trends to that observed in the $\pm 67.5^\circ$ specimen tests. However, the $\pm 67.5^\circ$ specimen is the preferred specimen for this sort of test, as scatter seems to be minimised for this test specimen configuration [1]. The procedure of determining the Ladevèze transverse damage and coupling parameters from a cyclic test of a 45° off-axis specimen is the same as the procedure described for the $\pm 67.5^\circ$ specimen with the exception of the equations used to determine the transverse and shear stresses and strains in the specimen. The transverse stress and shear stress are calculated from:

$$\sigma_{22i} = \tau_{12i} = \frac{\sigma_{Li}}{2} \quad (4.28)$$

where the symbols have the usual meanings

The transverse strains and shear strains were calculated from;

$$\varepsilon_{22i} = \varepsilon_{Li} + \varepsilon_{Ti} \quad (4.29)$$

$$\gamma_{12i} = \varepsilon_{Li} - \varepsilon_{Ti} \quad (4.30)$$

where the symbols have the usual meanings.

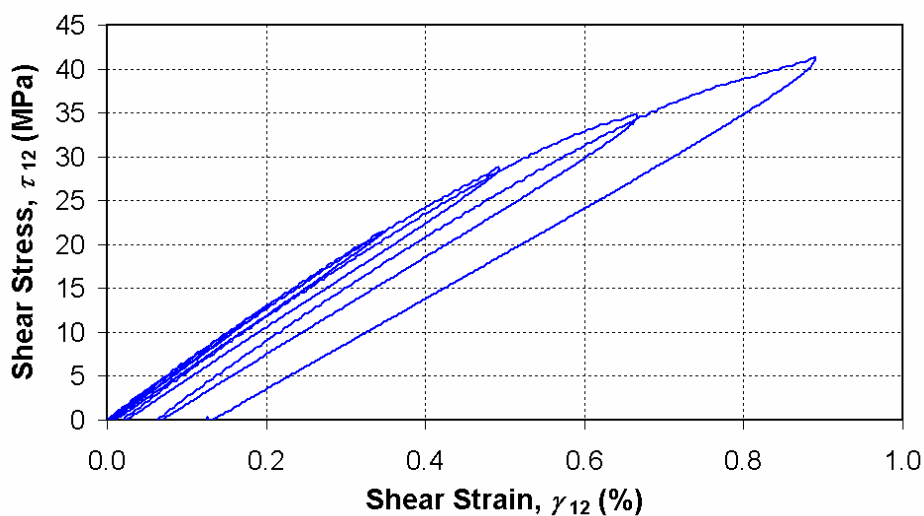


Figure 2.10 Typical shear behaviour for a cyclic tensile test on a HTA 6376 45° off-axis specimen.

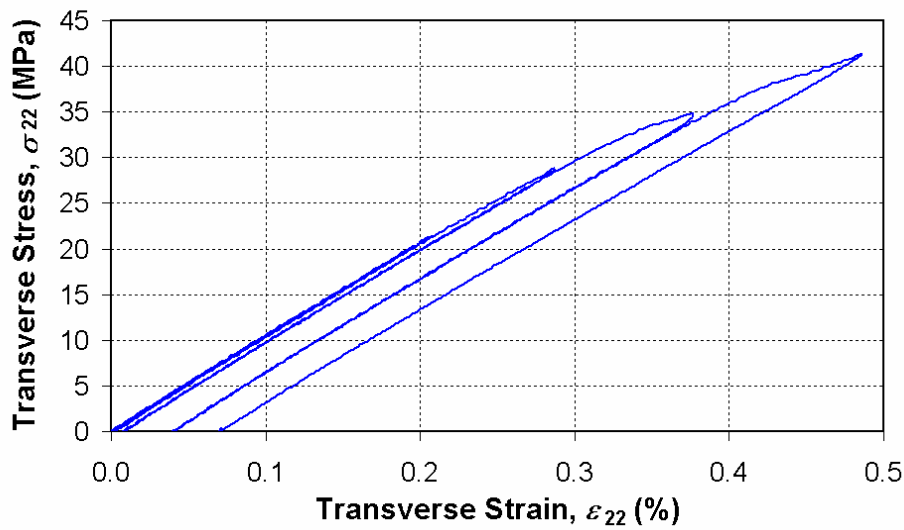


Figure 2.11, Typical transverse behaviour for a cyclic tensile test on a HTA 6376 45° off-axis specimen.

Figure 2.12 shows the transverse tension damage master curve, approximated from experimental data, for HTA 6376 CFRP. When compared with the transverse tension damage curve obtained from the $\pm 67.5^\circ$ test specimen, shown in figure 2.9, it is clear that there is far more scatter apparent in the data obtained from the 45° off-axis specimen tests. Tables 2.7 and 2.8 present the results obtained from tensile cyclic testing of the 45° off-axis specimens for the transverse damage master curve constants and the coupling factors, respectively, according to the procedure outlined in Section 2.2.3 above.

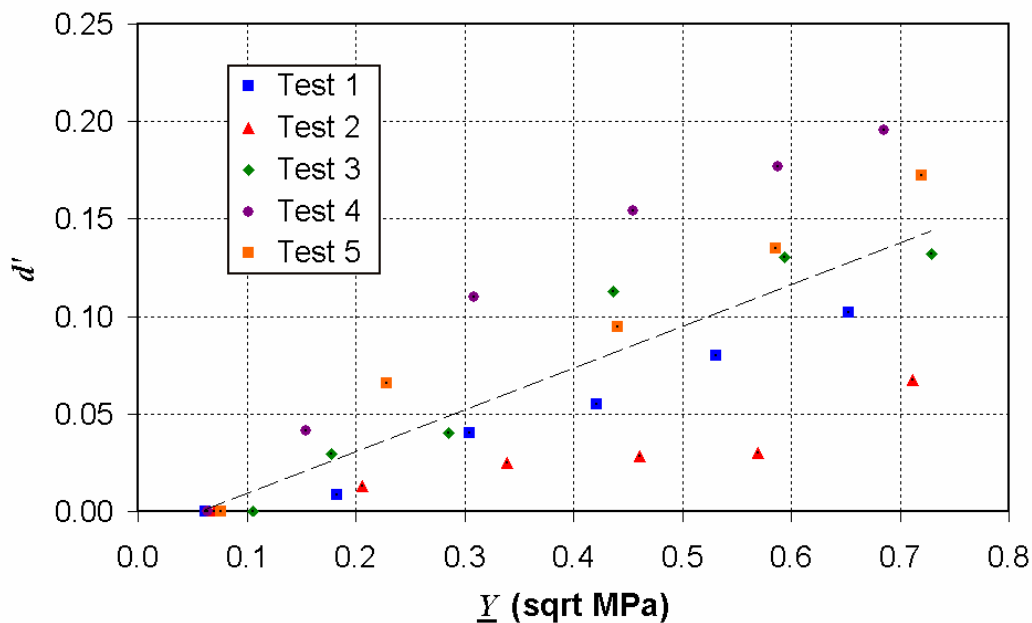


Figure 2.12 Transverse tension damage master curve for an elementary ply of HTA 6376 CFRP derived from 45° off-axis specimen tests

Table 2.7 Ladevèze model transverse damage master curve constants for HTA 6376 CFRP obtained from 45° off-axis specimen tests

Material System	Y'_0 ($\sqrt{\text{MPa}}$)	Y'_c ($\sqrt{\text{MPa}}$)
HTA 6376	0.18	2.91

Table 2.8 Ladevèze model damage and plasticity coupling factors for HTA 6376 CFRP obtained from 45° off-axis specimen tests

Material System	b	a^2
HTA 6376	2.69	0.88

From comparison of results for the Ladevèze parameters for both test specimens, as shown in table 2.9, it is clear that there is a significant difference between the results obtained by the $\pm 67.5^\circ$ cyclic tests and the 45° off-axis cyclic tests, particularly for the coupling parameters. According to Ladevèze and Le Dantec [1] this should not be the case. However, this difference can probably be attributed to the higher degree of scatter in the test data obtained from the 45° off-axis specimens. Figures 2.12 shows significant scatter in the data between individual tests obtained from 45° off-axis specimens. The significant scatter displayed for this test configuration suggests that the parameters obtained from these tests should not be relied upon.

Table 2.9 Comparison of coupling and transverse tension damage parameters obtained from $\pm 67.5^\circ$ and 45° off-axis cyclic tests

Parameters	HTA 6376	
	$\pm 67.5^\circ$	45°
Y'_0 ($\sqrt{\text{MPa}}$)	0.07	0.18
Y'_c ($\sqrt{\text{MPa}}$)	2.75	2.91
b	0.53	2.69
a^2	0.54	0.88

2.3 Conclusions

Ladevèze model parameters have been determined for an elementary ply of HTA 6376 CFRP according to the method outlined by Ladevèze and Le Dantec [1]. Basic material properties and model parameters in the fibre direction were accurately determined for tension loading conditions. Accurate shear damage and plasticity parameters were obtained from cyclic tensile testing of $\pm 45^\circ$ laminates. However, tests to determine transverse damage and coupling parameters from cyclic testing of $\pm 67.5^\circ$ and 45° off-axis laminates produced conflicting

results. Significant scatter was observed in test data obtained from 45° off-axis specimens for both material systems, indicating that this may not be a suitable test configuration for determining transverse damage and coupling parameters for the Ladevèze damage model. On the other hand, test data obtained from $\pm 67.5^\circ$ specimens was found to contain far less scatter indicating that this is a very suitable test configuration for determining transverse damage and coupling parameters. With this complete set of data, finite element numerical analysis can be carried out to calibrate a Ladevèze damage model for the prediction of damage growth and failure in laminates containing a through thickness open hole subjected to a tensile load. Table 2.10 contains all the parameters determined from this test series.

Table 2.10 Ladevèze damage model parameters

Material	HTA 6376
E_{11} (GPa)	133
E_{22}^0 (GPa)	10.1
G_{12}^0 (GPa)	6.11
ν_{12}^0	0.32
ε_{11} (%)	1.5
Y_c ($\sqrt{\text{MPa}}$)	3.10
Y_0 ($\sqrt{\text{MPa}}$)	0.048
Y'_c ($\sqrt{\text{MPa}}$)	2.75
Y'_0 ($\sqrt{\text{MPa}}$)	0.07
b	0.53
R_0 (MPa)	21.59
β (MPa)	558
m	0.38
a^2	0.54

Section 3: Calibration of Composite Open Hole Tension Ladevèze Damage Model in Pam-CRASH

The aim of this section is to present the work carried out at the University of Limerick to calibrate a Ladevèze Damage Model for fibre-reinforced composite open hole tension laminates in the ESI software package Pam-CRASH. A numerical study was carried out using existing code within Pam-CRASH; damage parameter input data obtained from the test series described in section two of this report. The Ladevèze Damage Model was implemented in Pam-CRASH using multi-layered shell element Material Type 131 in conjunction with the unidirectional composite global ply model (ITYP=1). An attempt was also made to implement delamination in the model using multiple layers of Material Type 131 shell elements bonded together using Material Type 303 (TIED Interface).

3.1 Model Properties

3.1.1 Geometry

A number of open hole tension laminates of varying ply lay-ups were examined during the course of the study. All laminates examined had the same basic geometry, i.e. 36 mm wide, 150 mm gauge length and a 6 mm hole in the centre of the laminate. However, the thickness varied according to the number of plies contained in the laminate, each ply had a thickness of 0.125 mm, laminates examined contained anything from four to twenty plies. Obviously, analysis of thick laminate models used more CPU time due to their greater complexity, therefore, most parameter studies were carried out on laminates with thickness in the region of four to eight plies to minimise the model CPU time for each analysis.

All models run in this study were quarter laminate models of the experimental open hole tension specimens, as shown in figure 3.1. The quarter laminate model was used as it was assumed that all stresses and strains were symmetrical about the x-axis and y-axis through the centre of the hole. Using the quarter model of the laminate further reduced the model CPU time for each analysis.

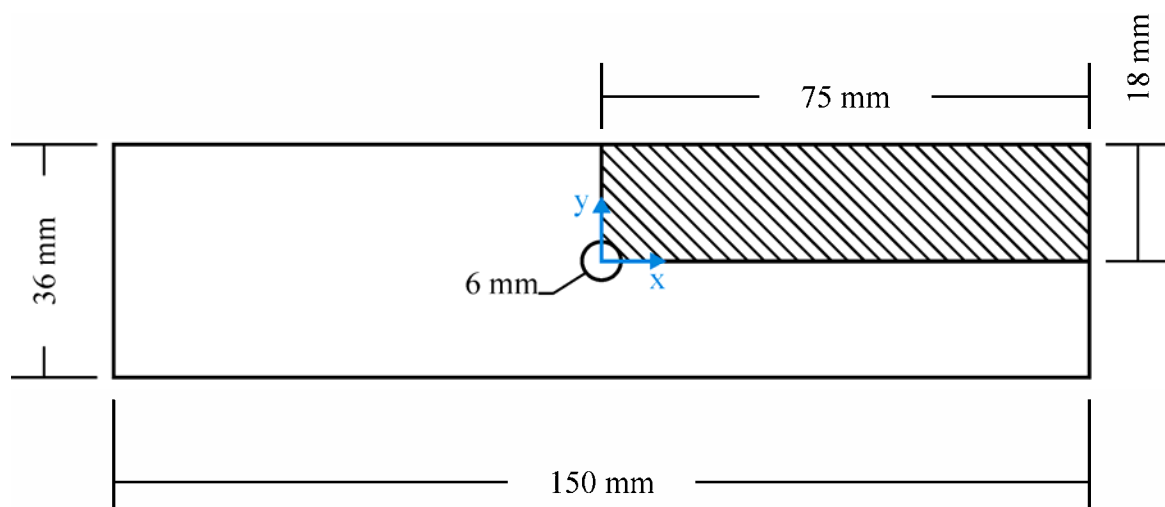


Figure 3.1, The open hole tension laminate geometry, the hatched area indicates the quarter laminate model section used in the FE study

3.1.2 Boundary Conditions

The quarter laminate model was subjected to three sets of boundary conditions, two sets of constraining boundary conditions and one loading boundary condition. The first set of constraining boundary conditions was applied to all element nodes on the edge of the quarter model at the cut along the y -axis. These element nodes were free to translate in the y direction, but were constrained in the x and z directions, in addition the nodes were constrained from rotation about any axis. The second set of constraining boundary conditions was applied to all element nodes on the edge of the quarter model at the cut along the x -axis. These elements were free to translate in the x direction, but were constrained in the y and z directions, in addition the nodes were constrained from rotation about any axis. The model was loaded by applying a velocity profile in the x direction to the element nodes along the edge of the quarter model at the opposite end of the model to the hole. Velocity profiles usually consisted of a rapid linear acceleration to the desired velocity, which was held for a period of time. The period of time for which the model was subjected to the velocity was dependent on how great a displacement one wanted to subject the model to. Figure 3.2 shows a schematic of the boundary conditions applied to the quarter model.

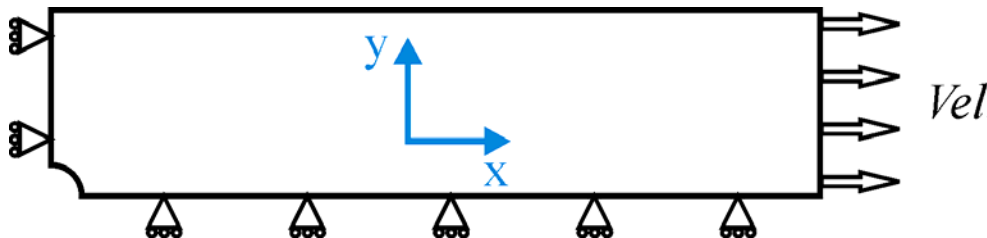


Figure 3.2, Schematic of the boundary conditions applied to the quarter laminate model

3.1.3 Output Data

In order for the quarter model to be accurately compared with the experimental data for open hole tension laminates, two user defined data output functions were used in the model. The nodal time history output function (THNOD_/_) was used to plot displacement in the x direction of an element node situated on the outer edge of the quarter laminate model, 12.5 mm from the edge cut along the y -axis. This point coincided with the approximate location of an extensometer blade on the open hole tension experimental specimens. In the experimental work the extensometer had a gauge length of 25mm which was placed on the edge of the laminate so that the centre of the hole coincided with the centre of the extensometer gauge length, therefore, the displacement of the node in the quarter model represents half the displacement of the extensometer in the experiment.

The cross section for force output function (SECFO_/_) was used to plot the reaction force at the edge of the quarter model at the cut along the y -axis. As this edge represents only half of the full laminate cross-sectional area, the reaction force obtained from the model represents half of the reaction force experienced by the experimental specimen. Using the outputs obtained from both of these functions, full load-displacement curves were plotted for each analysis run on the quarter laminate model, which were plotted against experimental data to check the accuracy of the model.

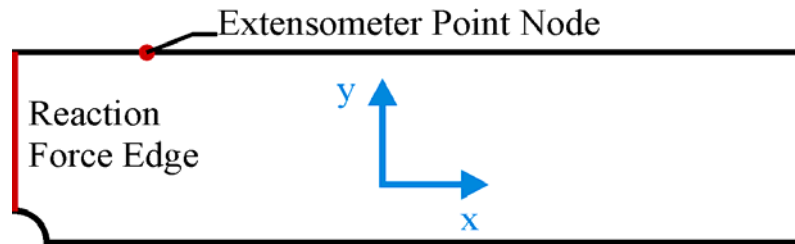


Figure 3.3, Schematic of quarter laminate model output data points

3.1.4 Quarter Laminate Model Element Mesh

All parameter studies carried out on the quarter laminate model used the same element mesh shown in figure 3.4. This mesh is made up of quadrilateral thin shell elements (SHELL_/_). The mesh was relatively fine, with particular refinement around the open hole area as this is the area of most interest. All element aspect ratios were found to be within acceptable limits. Such a fine mesh did increase the model CPU for each analysis, as the time step is dependent on the size of the smallest element. However, a fine mesh was considered necessary to represent some of the physical phenomena observed in the tests (e.g. axial splits in the longitudinal plies), and also for use of the delamination model in later studies.

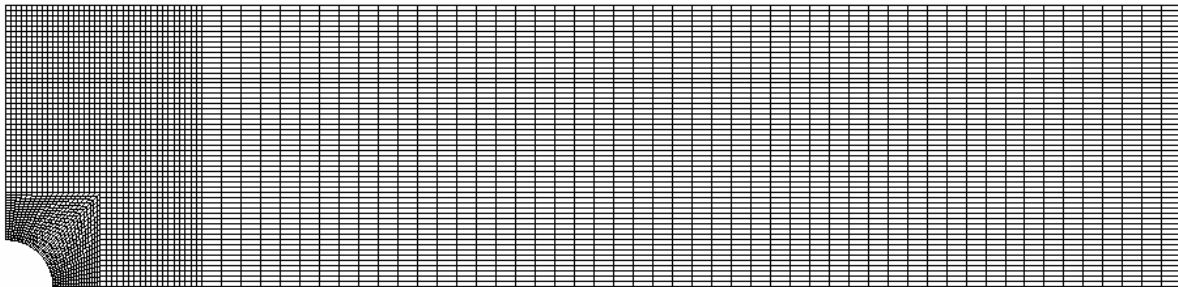


Figure 3.4, Quarter laminate model element mesh

3.2 Parameter Studies

Early on in the numerical study, it became apparent that the velocity, which was applied to the quarter laminate model to induce a displacement in the model, had an effect on the results of the model, and the CPU time for the model analysis. It was therefore decided to run a number of parameter studies to try to improve the accuracy of the model, while keeping CPU time to an acceptable level.

3.2.1 Effect of Velocity Profile

As mentioned previously, velocity profiles were used to induce displacements in the FE model. All velocity profiles used consisted of rapid linear acceleration from rest to a desired velocity, which was maintained for a period of time to induce a desired displacement in the model. To study the effect of velocity on the accuracy of the model a short study was carried out. To induce a model displacement of 2 mm, five different velocities were used, namely, 40, 20, 10, 5 and 2 m/s. A cross-ply laminate ($CP_3 = [90/0]_{2s}$) consisting of eight plies was modelled in the study. Load-deflection curves plotted from the output data obtained for each of the velocities are presented and compared with experimental data in figure 3.5. It can

clearly be seen that the velocity profile applied in the model has a significant affect on the accuracy of the model. It is noted that for the higher velocities a significant lag in load pick-up is introduced (due to inertia effects) and the stiffness of the model is much higher than in the experiment. Lower velocity gives a good representation of the stiffness, but the failure load is drastically underpredicted.

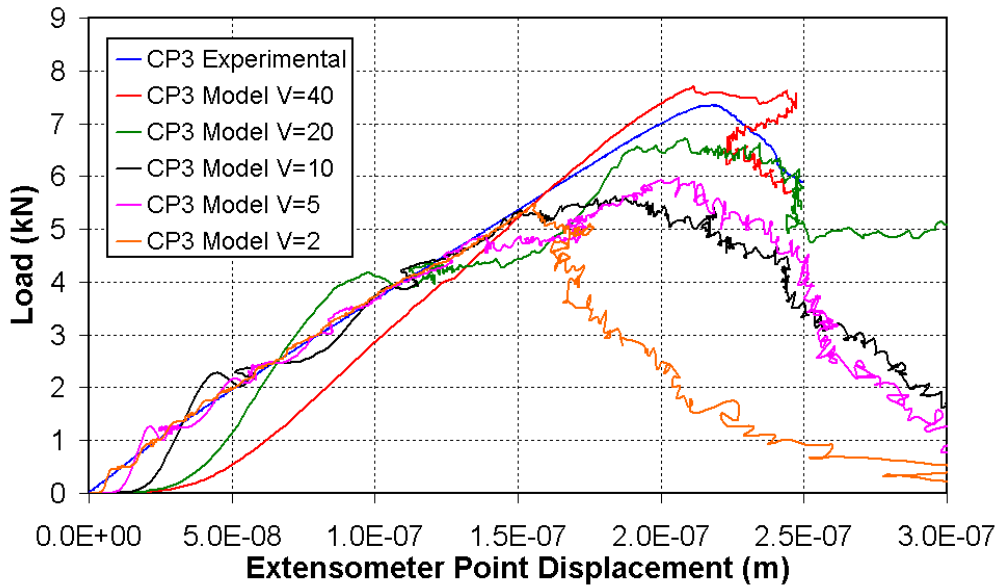


Figure 3.5, The effect of velocity on the accuracy of the quarter laminate model

In addition, as part of this study, the effect that the initial rapid linear acceleration part of the velocity profile had on the model was examined. Four different accelerations to 40m/s^2 were investigated. However, as can be seen from the results plotted in figure 3.6, changing the ramp acceleration of the velocity profile did not appear to have a significant affect on the results of the model.

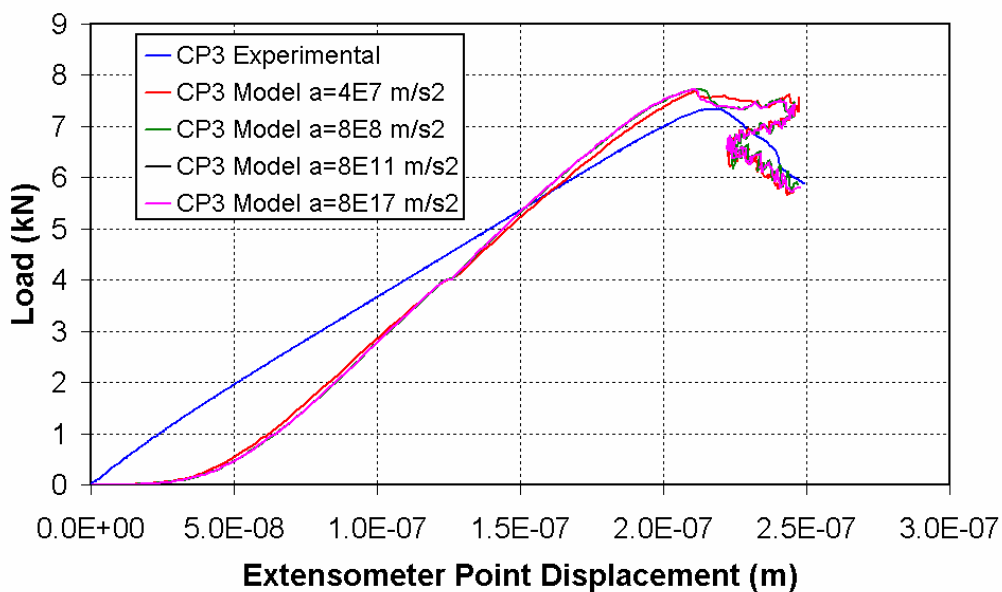


Figure 3.6, The effect of the velocity profile ramp acceleration on the stability of the quarter laminate model

3.2.2 Model Study Using an Applied Velocity of 2m/s

Having established that the velocity applied to the model significantly affects the model stiffness; it was decided to run a number of models at 2m/s to determine if accurate, practical FE analyses could be achieved by applying this relatively low velocity (note: even this velocity is 67000 times the experimental velocity of 0.03mm/s). Four open hole laminate models of varying thickness and lay-up were run. The laminate lay-ups in question were cross-ply CP₃ ([90/0]_{2s}) and CP₄ ([90₂/0₂]_s), quasi-isotropic QI ([45/0/-45/90]_{2s}) and zero-dominated ZD₁ ([45/0/-45/90/0/0/45/0/-45/0]_s). The CP₃ and CP₄ laminates both have a thickness of 8 plies, while the QI and ZD₁ laminates had 16 and 20 plies respectively. Results from each analysis are presented in figure 3.7. It is clear that each of the models run with a 2 m/s applied velocity give reasonably good agreement in terms of stiffness with the experimental data. However, all models significantly under predict the failure strengths of the open hole laminates. In addition, the model CPU times were impractical; the CP₃ and CP₄ models have CPU times of 4 hours 23 minutes and 4 hours 10 minutes, respectively. The operator terminated both the QI analysis and the ZD₁ analysis before being fully completed as they were deemed to be running for too long. It was felt that long model run times such as this were highly impractical for the detailed parameter study which would have to be carried out to fully calibrate the damage model. Clearly, the effect which applied velocity had on accuracy of models was due to inertia effects within the models. It was decided to do further parameter studies in an effort to determine a way of reducing model runtime while maintaining a reasonably degree of model accuracy.

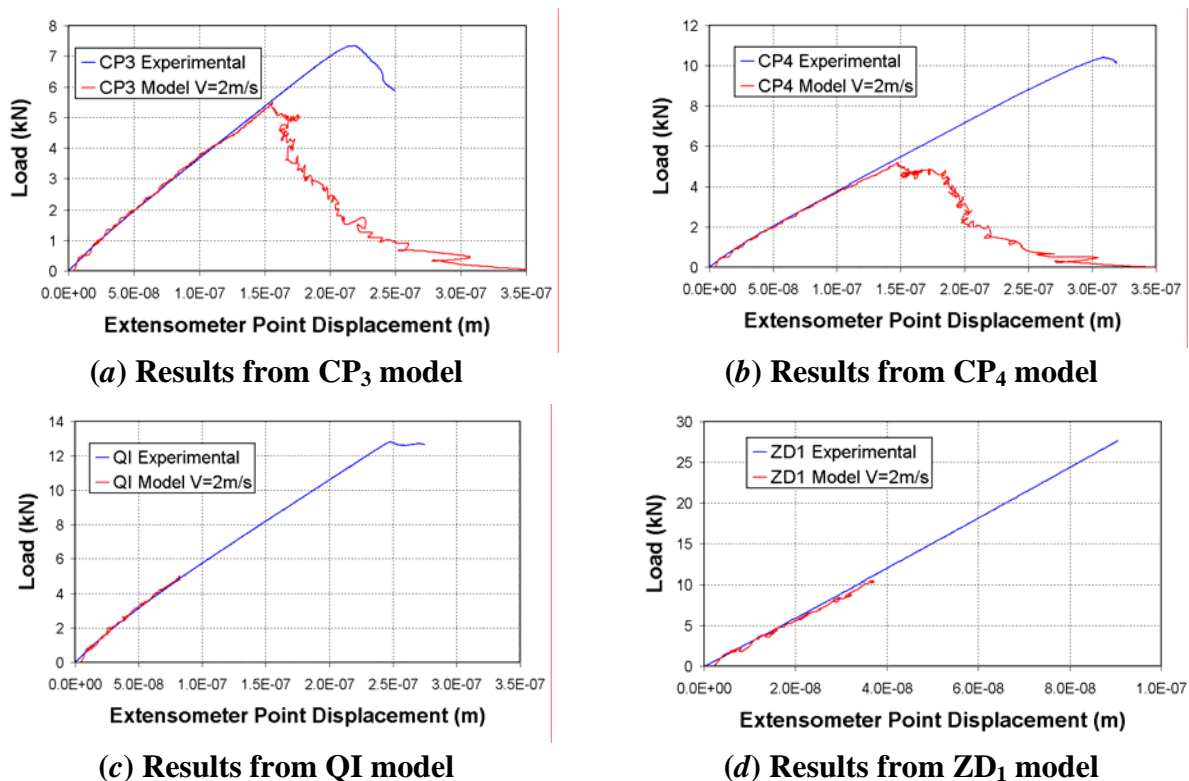


Figure 3.7, Comparison of results from models with a 2m/s applied velocity with experimental data

3.2.3 Effect of Material Density

As inertia effects affected the model, it was decided to do a study of the effect of material density. As no density had been experimentally determined for the HTA 6376 CFRP material, the initial density used for all models was 1550 kg/m^3 , which was a value that had been used previously when modelling fibre-reinforced composites in Pam-CRASH. This value of density was used as the base value for the present parameter study and all other densities are given as a percentage of this base value. All analysis was carried out on the CP4 ($[90_2/0_2]_s$) open hole laminate quarter model. To try to ensure reasonable runtimes, an applied velocity of 20 m/s was used for each analysis. Figure 3.8 presents the results of varying material density. Clearly, increasing the density only increases the inertia effects in the model. However, decreasing the density decreases the model inertia effects and clearly gives better agreement with experimental data in terms of stiffness. However, this gain in accuracy is again achieved at the sacrifice of significantly longer analysis CPU time as shown in figure 3.9.

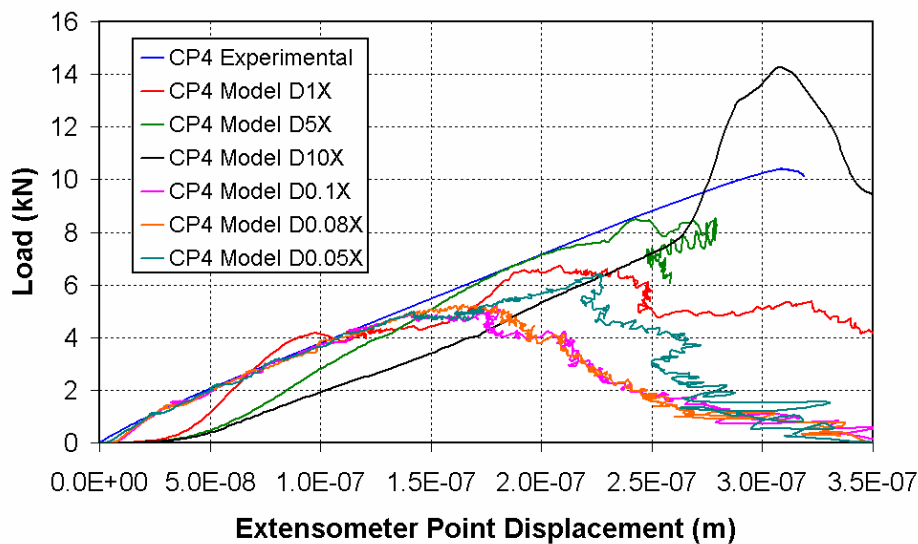


Figure 3.8, Comparison of the effect of varying input density on model stability

Note: D represents the base density 1550 kg/m^3 , D#X represents the multiple of the base density

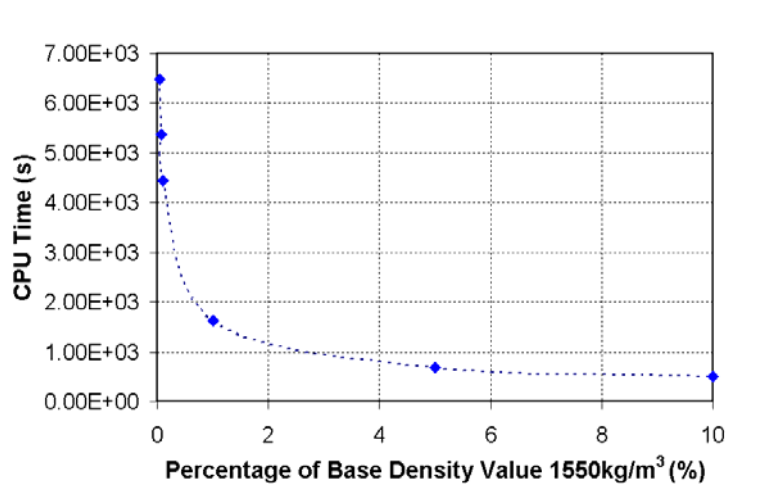


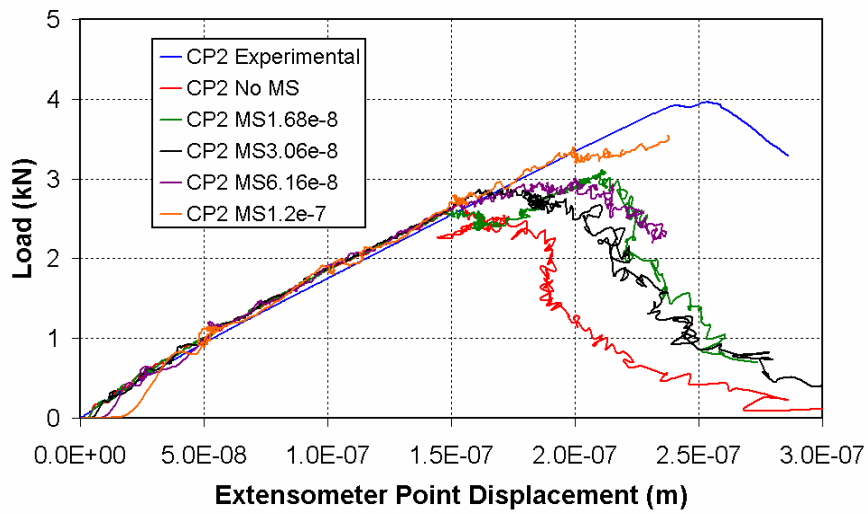
Figure 3.9, Comparison of input density with model analysis CPU time

3.2.4 Effect of Mass Scaling

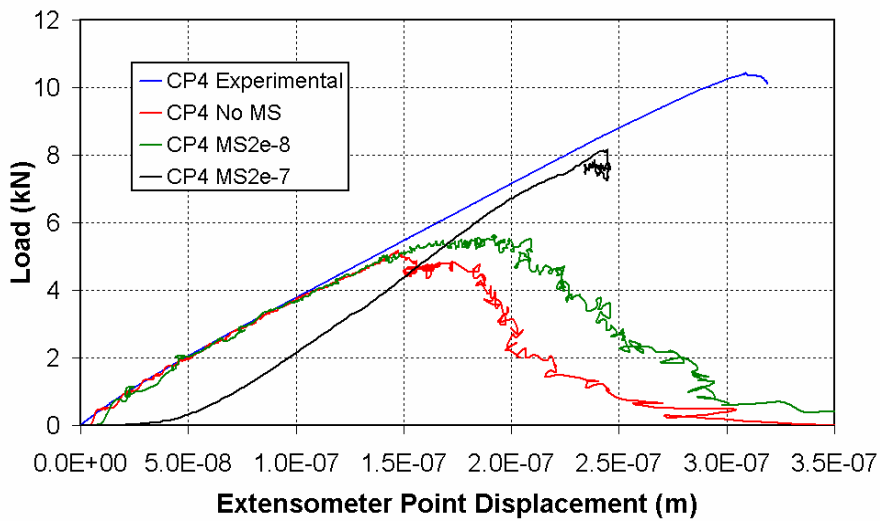
An alternative method of reducing the model inertia effect is to use the mass scaling function within Pam-CRASH (INIT_MASS_SCALE). This function is activated when the operator specifies a time-step for the analysis run (parameter DTSCAL), if the time-step of the smallest element is found to be less than the input time-step value the mass scaling algorithm is activated and the programme adjusts its mass density such that its time step equals that input by the operator. The effect of mass scaling was investigated for three different laminate lay-ups; viz. CP₂, ([90/0]_s), CP₄ ([90₂/0₂]_s) and ZD₁ ([45/0/-45/90/0/0/45/0/-45/0]_s). These lay-ups were chosen for their varying thickness, CP₂ has only 4 plies and therefore has a relatively quick analysis CPU time. CP₄ and ZD₁ having 8 and 20 plies, respectively, are more representative of the type of lay-ups under examination and any reduction in their analysis CPU time while maintaining model accuracy would have significant implications for the numerical study overall. The velocity applied to the models was 2 m/s to help ensure that the most accurate results are obtained from each analysis in terms of stiffness. The time steps input for each analysis carried out with the mass scaling algorithm were multiples of the time step of the smallest element in each model.

Figure 3.10 presents the results for each analysis of the different lay-ups. It is clear that implementing mass scaling doesn't appear to affect the accuracy of the results obtained from the model as long as the time step input by the operator is a relatively small multiple of the time step of the smallest element in the model. However, if the time step input is too large, the accuracy of the model can be significantly affected.

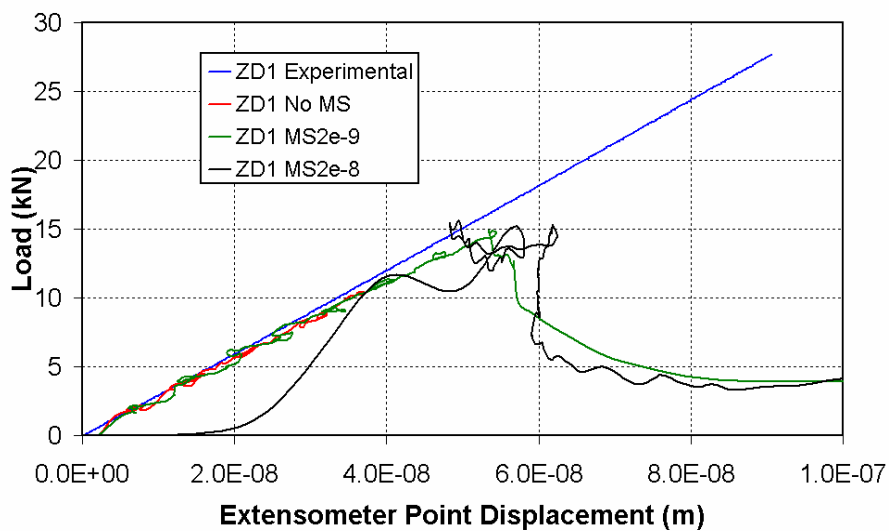
Upon examination of the *.out report files for each analysis it was found that implementing the mass scaling algorithm significantly reduces the analysis CPU time, e.g. for the CP₂ model using the mass scaling algorithm to change the time step from 3.065e-9s to 1.68e-8s reduced the analysis CPU time from approximately 1 hour 28 minutes to just 17 minutes without significantly reducing the accuracy of the model. However, although mass scaling appears to work in significantly reducing CPU time without significantly increasing model inaccuracies, values for input time-step cannot just be arbitrarily chosen. Model accuracy is dependent on the size of the time step chosen and varies from model to model. Parameter studies must be carried out for each model to determine the optimum time step for use with the mass scaling algorithm so that the correct balance is achieved between model accuracy and practical analysis CPU time.



(a) Results from the CP₂ model



(b) Results from the CP₄ model



(c) Results from the ZD₁ model

Figure 3.10, Comparison of the effect of mass scaling on model accuracy

3.3 Delamination Modelling

In the course of an open hole tension laminate experimental test series, carried out at the University of Limerick, two laminates with similar cross-ply lay-ups, but with different stacking sequences were tested; viz. CP₃, [90/0]_{2s}, and CP₄, [90₂/0₂]_s. The CP₄ laminate was found to be significantly stronger than the CP₃ laminate even though both contained an equal number of primary load bearing 0° plies and supporting 90° plies. From experimental examination it was concluded that the block stacking of 0° plies in the CP₄ open hole laminate allowed axial splits to occur more easily in 0° plies, accompanied by large regions of triangular delamination from the tips of the splits to the edge of the hole. This was resisted by the alternating stacking sequence of the 0° plies and 90° plies in the CP₃ laminate. This damage formation prior to failure blunted the stress concentration at the hole and hence increased the overall strength of the laminate.

Both the CP₃ and CP₄ open hole laminates were modelled using multi-layered shell element Material Type 131 in conjunction with the unidirectional composite global ply model (ITYP=1). However, as can be seen in figure 3.11, no significant difference was noticed between the results of the models of each laminate.

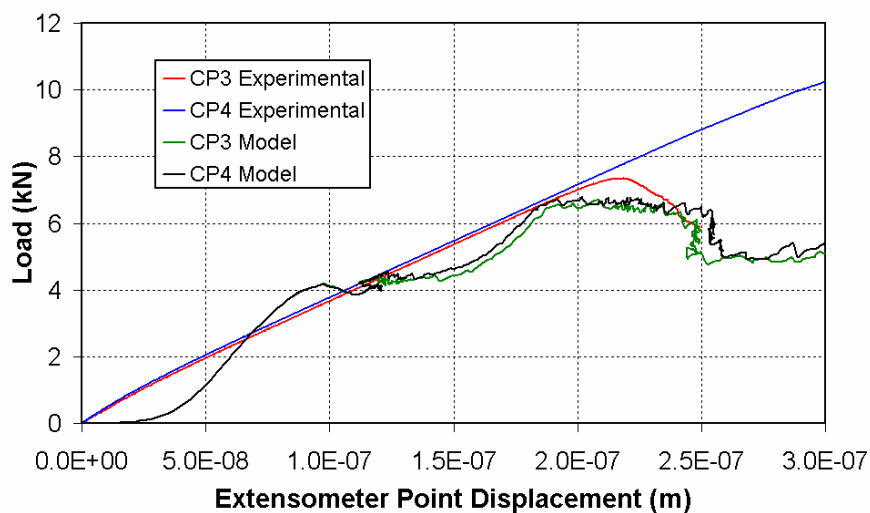


Figure 3.11, Comparison of results from CP₃ and CP₄ multi layer shell element models (applied velocity of 20m/s)

A delamination model was implemented in Pam-CRASH for both CP₃ and CP₄, using multiple layers of Material Type 131 shell elements bonded together using the Material Type 303 (TIED Interface). Input data for Material Type 303 was obtained from a delamination model for HTA 6376 CFRP material developed at the University of Limerick. However, as with the results from the multi-layer shell elements, no significant difference was noticed between the results of the models of each laminate, as shown in figure 3.12. In fact, the results obtained from the delamination models do not appear to be as accurate as the results obtained from the multi-layer shell element models, relative to the experimental results. A brief parameter study was made of the variable inputs for Material Type 303, however, no significant improvement in results was achieved and it was decided to abandon delamination modelling and concentrate on calibrating the damage model using only the multi-layer shell elements.

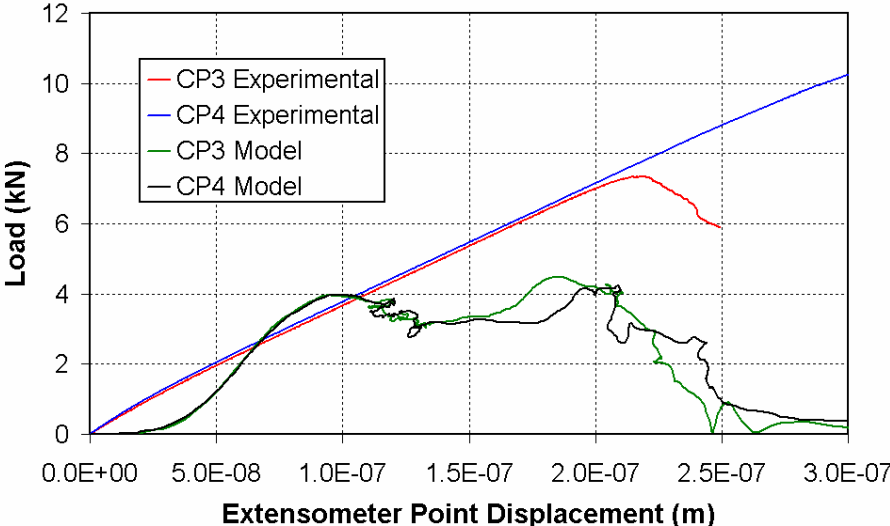


Figure 3.12, Comparison of results from CP₃ and CP₄ delamination models (applied velocity of 20m/s)

4.0 Conclusions and Recommendations

In spite of numerous parameter studies, to try to increase the accuracy of the damage model, the hoped for results were not achieved in this numerical study. Reasonably good agreement in terms of stiffness was achieved in some models. However, all models significantly under predicted the failure strength of the open hole tension laminates. In addition, problems associated with model inertia effects were not solved sufficiently to allow the model to be considered useful for practical applications. Unfortunately, the problems associated with trying to model quasi-static experiments with an explicit finite element code were considered too great to try to overcome in the short time frame allocated for this project and so further work using Pam-CRASH has been stopped for now, and work is progressing with an implicit code.

A set of Ladevèze damage model parameter data has been supplied in this report, unfortunately, results obtained from the numerical study were insufficiently accurate to fully validate the usefulness of this data. However, it is recommended that single element models be used, within the Pam-CRASH finite element code, to validate this data.

5.0 References

1. Ladevèze, P. & E. Le Dantec, “Damage Modelling of the Elementary Ply for Laminated Composites”, *Composites Science and Technology*, vol.43, pp. 257-267, 1992.
2. ASTM Standard D3039/D3039M – 00, “Standard Test Method for Tensile Properties of Polymer Matrix Composite Materials”, 2000.
3. ASTM Standard D5687/D5687M – 95 (2002), “Guide for Preparation of Flat Composite Panels with Processing Guidelines for Specimen Preparation”, 2002.

6.0 Acknowledgements

The authors would like to thank all at ESI Software for their sponsorship of this project and the technical support provided for its duration.